Hindawi
Journal of Nanomaterials
Volume 2021, Article ID 9991050, 13 pages
https://doi.org/10.1155/2021/9991050

Research Article

Fluoride and Arsenite Removal by Adsorption on La_2O_3-CeO_2/Laterite

Duong Thi Lim,[1] Trinh Ngoc Tuyen,[1] Dao Ngoc Nhiem,[2,3] Dao Hong Duc,[3] Pham Ngoc Chuc,[2] Nguyen Quang Bac,[2,3] Dang Xuan Tung,[4] Ngo Nghia Pham,[5] Luu Thi Viet Ha,[6] Nguyen Thi Thanh Tu,[7] Vo Thang Nguyen,[8] and Dinh Quang Khieu[9]

[1]*Institute of Geography, VAST, 10000, Vietnam*
[2]*Institute of Material Science, VAST, 10000, Vietnam*
[3]*Graduate University of Science and Technology, VAST, 10000, Vietnam*
[4]*Institute of Geological Science, VAST, 10000, Vietnam*
[5]*VNU University of Science, 10000, Vietnam*
[6]*Industrial University of Ho Chi Minh City, 70000, Vietnam*
[7]*Van Lang University, 70000, Vietnam*
[8]*University of Education and Science, The University of Danang, 50000, Vietnam*
[9]*University of Sciences, Hue University, 53000, Vietnam*

Correspondence should be addressed to Dao Ngoc Nhiem; nhiemdn@ims.vast.ac.vn
and Dinh Quang Khieu; dqkhieu@hueuni.edu.vn

Received 5 April 2021; Accepted 26 June 2021; Published 21 July 2021

Academic Editor: Dong kee Yi

In the present article, the adsorbent prepared from laterite with lanthanum and cerium oxides (La_2O_3-CeO_2/laterite (LCL)) was efficiently employed for the removal of arsenite and fluoride from an aqueous environment. The obtained materials were characterized by XRD, SEM, and nitrogen adsorption/desorption. The synthesized LCL exhibited a high adsorption capacity towards arsenite (As(III)) and fluoride. The adsorption of both analytes on LCL, which was well-fitted to a *pseudo*-second-order equation, was found to be kinetically fast in the first 20 minutes and reached equilibrium at around 180 minutes. Weber's intraparticle diffusion model in multilinearity using the piecewise linear regression combined with Akaike's criteria was addressed. The adsorption capacities of LCL calculated from Langmuir's isotherm model were found to be 67.08 $mg{\cdot}g^{-1}$ for arsenite and 58.02 $mg{\cdot}g^{-1}$ for fluoride. Thermodynamic parameters presented an endothermic nature of arsenite adsorption but an exothermic nature for fluoride and a negative Gibbs free energy for the spontaneous process of arsenite or fluoride adsorption at the studied temperature range. The excellent adsorption performance and stability make the composite of laterite and La-Ce binary oxides an alternative efficient and cheap adsorbent for the removal of arsenite and fluoride in an aqueous solution.

1. Introduction

Arsenic or fluoride-contaminated water is an environmental problem which can lead to severe human health implications and ecological concern [1, 2]. These elements are increasingly introduced to water sources by natural processes or human activities [3, 4]. Inorganic species of arsenic in both forms of arsenate (As(V)) and arsenite (As(III)) prevail in groundwater. However, its valence states depend on the redox environment in aqueous sources and may change from region to region, in which arsenite is considered more mobile and acutely toxic than arsenate [5]. The acceptable concentration is 10 $\mu g{\cdot}L^{-1}$ for total arsenic in drinking water [6, 7]. Excess arsenic in drinking water can cause some health problems such as neurological complications, skin lesions, kidney cancers, and the retardation of mental development of children [8]. Meanwhile, fluorine is abundant in the natural environment which is released from the fluoride-containing minerals

and wastewater discharge from industrial processes using fluorine compounds [9]. It can be introduced into the human body via food and water consumption [10]. It is advised that the fluoride concentration in the range 0.5–1.5 mg·L^{-1} is acceptable in drinking water [11]. A higher concentration will have negative effects on the metabolism of several elements such as P and Ca in the human body and can cause dental fluorosis or molting of teeth [12]. Fluoride concentration, however, has been found to exceed the permissible values in groundwater in many regions in the world, especially in developing countries.

Some studies have reported that arsenic or fluoride elimination can be achieved by various methods such as oxidation/precipitation [13, 14], electrocoagulation [15], reverse osmosis and nanofiltration [16, 17], ion-exchange resin [18], polymer ligand exchange [19], coagulation and microfiltration [20], dialysis [21], ion-exchange processes [18], and adsorption processes [22]. Each method has its own advantages; however, the adsorption process is still considered one of the most employed techniques due to its low cost and simple operation without the use of large amounts of chemicals or the discharge of contaminated coagulant sludge as found in other methods. Therefore, the search for new and economical adsorbents with high adsorption capacity and affinity for contaminated elements that can be effectively employed under relevant environmental conditions has recently attracted extensive attention from scientists. Natural iron-contained minerals such as diatomite, laterite, kaolinite, montmorillonite, and illite are highly effective and widely used to remove arsenic [23, 24]. Among them, the laterites are promising alternative adsorbents in removing hazardous anions because of their high surface area and abundant number of adsorptive sites. Laterites are found from the weathering of parent rocks in tropical climate regions with their chemical composition varying according to the nature of parent rocks. Laterites are predominantly composed of quartz, aluminum hydroxide, kaolinite mineral, goethite, and hematite [23] and are abundantly available in several regions in the central and northern areas of Vietnam. Recently, synthesized nanosized adsorbents including La_2O_3, Fe_3O_4, CeO_2, CuO, MnO_2, and TiO_2, which exhibited a potential ability to remove arsenic or fluoride from an aqueous environment, have been extensively studied [25–27]. Their improved adsorption could be attributed to their controllable surface properties, being suitable for arsenite and fluoride removal. Cerium and lanthanum oxides or their binary oxides have been studied for application in areas such as catalysts [28, 29], electrochemistry [30], and disease therapy [31] due to their specific physical and chemical properties. For environmental applications, cerium and lanthanum oxides have demonstrated a high adsorption capacity for hazardous chemical substances, such as arsenate [32], phosphate [33], and dyes [34]. Embedding such nanoparticles on laterite is expected to produce a promising adsorbent with low cost, yet great adsorption capacity for environmental remediation applications.

In the present work, the composite of low-cost natural laterite and La-Ce bimetal oxides (LCL) is explored as a potential fluoride and arsenic adsorbent. Both equilibrium and kinetic studies are conducted to evaluate the adsorption effectiveness of LCL to remove arsenite and fluoride from water. The Langmuir and Freundlich isotherms were addressed, and the thermodynamic calculations were also performed to have more insight into the process.

Table 1: Chemical composition of used laterite.

Oxides	%
Al_2O_3	40.69
SiO_2	14.38
Fe_2O_3	32.14
CaO	0.14
MgO	0.18
S	1.94
K_2O	0.33

2. Experiments

2.1. Materials. Laterite for this study was collected from the northern area of Vietnam. It was ground and washed several times by distilled water. After being dried, solids were screened and stored in a desiccator for further use. The oxide composition analyzed by the X-ray fluorescence method (XRF) is listed in Table 1.

Gelatin (Mw = 834), lanthanum nitrate hexahydrate ($La(NO_3)_3{\cdot}6H_2O$, 99%), and cerium nitrate hexahydrate ($Ce(NO_3)_3{\cdot}6H_2O$, 99%) were obtained from Merck (Germany). Other reagents were of analytical grade.

Arsenite and fluoride stock solution (1000 mg·L^{-1}) was prepared by dissolving sodium-meta-arsenite ($NaAsO_2$, Merck, Germany) and sodium fluoride (NaF Merck, Germany) in distilled water. The working solution was freshly prepared from stock solution (1000 mg·L^{-1}) to the desired concentration. The acid (0.01 M HNO_3) and base solutions (0.01 M NaOH) were employed for pH adjustments.

2.2. Synthesis of La_2O_3, CeO_2, and La_2O_3-CeO_2/Laterites (LCL). To synthesize La_2O_3 and CeO_2, gelatin (50 grams) was firstly dissolved in distilled water at 80°C before adding $La(NO_3)_3$ or $Ce(NO_3)_4$ at a $La(NO_3)_3$/gelatin or $Ce(NO_3)_4$/-gelatin molar ratio of 1/1. The mixture was stirred properly to form a gel. The obtained gel was dried at 110°C in 12 hours and calcinated at 550°C for 4 hours to generate the corresponding oxide. An LCL sample was synthesized in a similar manner, with the molar ratio of $La(NO_3)_3$/$Ce(NO_3)_4$/gelatin being 1/1/1. The pH of the mixture was adjusted to 7. Laterite was added at an oxide/laterite mass ratio of 10/90 just after gel formation. This mixture was then continuously stirred to allow an even dispersion of the gel over the laterite. Then, the laterite gel was dried at 110°C in 12 hours and finally calcined at 550°C for 2 hours to obtain LCL.

2.3. Apparatus. X-ray diffraction (XRD) was measured on a Bruker D8 ADVANCE with CuKα, $\lambda = 0.15406$ nm. The X-ray fluorescence spectrometer (XRF) used was a ZSX Primus IV (Rigaku, Japan). Thermal analysis (TG-DTA) was recorded

in an ambient atmosphere from room temperature to 850°C using a Setaram thermal analyzer (France). Energy-dispersive X-ray elemental mapping was performed on a Bruker D8 ADVANCE (Germany). The nitrogen adsorption/desorption isotherms were characterized by the Quantachrome Autosorb-iQ Station 1 (USA). The arsenic element was measured by atomic absorption spectroscopy (AAS) using a PerkinElmer Analyst 200 with an acetylene flame (F-AAS) at a wavelength of 193.7 nm. The fluoride concentration was measured with the spectrophotometric method using a vanadate-molybdate reagent according to Vietnam's standard (TCVN 6202:2008).

2.4. Adsorption Study

2.4.1. Kinetics, Thermodynamics, and Equilibrium Study of Adsorption Process

(1) Adsorption Kinetics. The adsorption capacity (q_t) and equilibrium adsorption capacity (q_e, mg·g^{-1}) were calculated as equation (1) and equation (2), respectively:

$$q_t = V\frac{C_o - C_t}{m}, \quad (1)$$

$$q_e = V\frac{C_o - C_e}{m}, \quad (2)$$

where V is the solution volume (L); m is the weight of the adsorbent (g); C_o, C_t, and C_e (mg·L^{-1}) are the concentrations of the adsorbate at the initial, certain, and equilibrium times.

The kinetics data were analyzed using the *pseudo*-first-order kinetic and *pseudo*-second-order kinetic models. The *pseudo*-first-order kinetic and the *pseudo*-second-order kinetic equations in the nonlinear form [35, 36] are written as equation (3) and equation (4), respectively:

$$q_t = q_e \cdot \left(1 - e^{-k_1 \cdot t}\right), \quad (3)$$

$$q_t = q_e \frac{q_e \cdot k_2 \cdot t}{1 + q_e \cdot k_2 \cdot t}, \quad (4)$$

where k_1 (min^{-1}) and k_2 (g·mg^{-1}·min^{-1}) are the rate constants for the *pseudo*-first-order kinetic and the *pseudo*-second-order kinetic models, respectively.

The values of k_1, k_2, and q_e were obtained by the nonlinear regression method with the Solver function in Microsoft Excel.

For the study of kinetics diffusion, the intraparticle diffusion model proposed by Weber and Morris [37] is used (equation (5))

$$q_t = k_i \cdot t^{1/2} + x_i, \quad (5)$$

where k_i (mg·g^{-1}·min$^{-0.5}$) is the intraparticle diffusion rate constant, x_i (mg·g^{-1}) is a constant related to the thickness of the boundary layer. The values of k_i and x_i were obtained from the slope of the linear plot of q_t versus $t^{1/2}$. If intraparticle diffusion is the rate limiting step, then a linear plot of q_t vs. $t^{0.5}$ will give an intercept equal to zero. Otherwise, the intraparticle diffusion is not the only rate-limiting step. The plot of Weber's model often consists of multilinearity in nature. A statistical approach of the piecewise linear regression combined with Akaike's criteria proposed by Malash and El-Khaiary [38] for the analysis of kinetics data was described in S1.

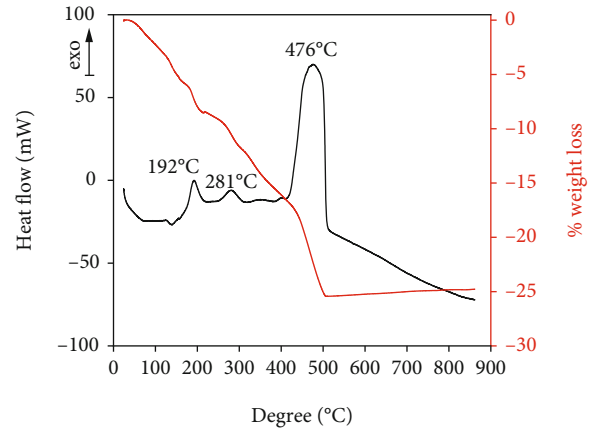

Figure 1: TG-DSC of as-synthesized La_2O_3/CeO_2/laterite.

(2) Thermodynamics Adsorption. Thermodynamic studies were performed in batch condition. LCL (2.5 g) was added to 500 mL of the arsenite solutions (5 and 10 mg·L^{-1}) and fluoride solutions (5 and 10 mg·L^{-1}) in a 1-litre beaker attached with a mechanical stirrer at room temperature. Four mL of the solution was withdrawn at different times. The concentration of arsenite or fluoride in the supernatant was determined by the corresponding analysis method.

The temperature effect on arsenite or fluoride adsorption was investigated using 0.5 g of LCL in a 100 mL flask containing arsenite solution (10 mg·L^{-1}) or fluoride solution (10 mg·L^{-1}). The flasks were magnetically stirred for 6 hours at a fixed temperature to obtain the adsorption/desorption equilibrium. The equilibrium concentration of arsenite or fluoride in the supernatant was measured. The distribution coefficient K_d is described as follows [39]:

$$K_d = \frac{C_o - C_e}{C_e}. \quad (6)$$

The change of standard Gibbs free energy of adsorption (ΔG°) is expressed by

$$\Delta G^\circ = \Delta H^\circ - T \cdot \Delta S^\circ, \quad (7)$$

where ΔG°, ΔH°, and ΔS° are the change of standard Gibbs free energy, enthalpy, and entropy.

The relationship between K_d and ΔH° and ΔS° can be demonstrated as follows:

$$\mathrm{Ln}K_d = -\frac{\Delta H^\circ}{R \cdot T} + \frac{\Delta S^\circ}{R}, \quad (8)$$

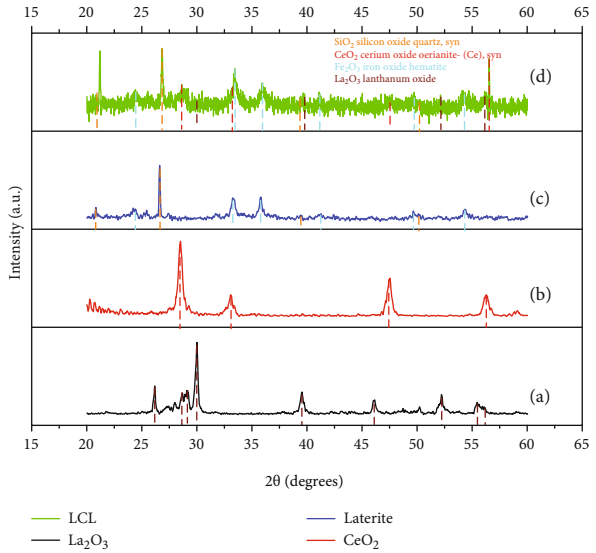

Figure 2: XRD patterns of (a) La_2O_3, (b) CeO_2, (c) laterite, and (d) LCL.

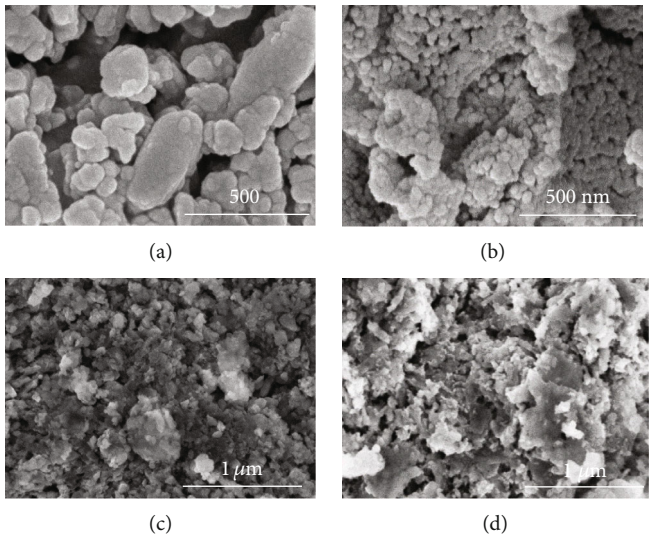

Figure 3: SEM observations of (a) La_2O_3, (b) CeO_2, (c) laterite, and (d) LCL.

The linear plot of $\ln(K_d)$ *vs.* $1/T$ provides the values of ΔH° and ΔS°.

(3) Equilibrium Study. The equilibrium study was performed at ambient temperature. Briefly, 0.5 g of adsorbent (LL, CL, and LCL) was introduced into eleven 200 mL flasks filled with 100 mL of different arsenite or fluoride concentrations (*i.e.*, 1, 5, 10, 20, 30, 40, 50, 100, 120, 150, and 200 mg·L^{-1}). The flasks were stirred by a shaker for 12 hours at room temperature. Afterwards, the liquid was obtained by centrifugation.

Two isotherm models of Freundlich and Langmuir were employed to analyze the equilibrium data. The Freundlich isotherm model is described as follows [40]:

$$q_e = K_F \cdot C_e^{1/n}, \quad (9)$$

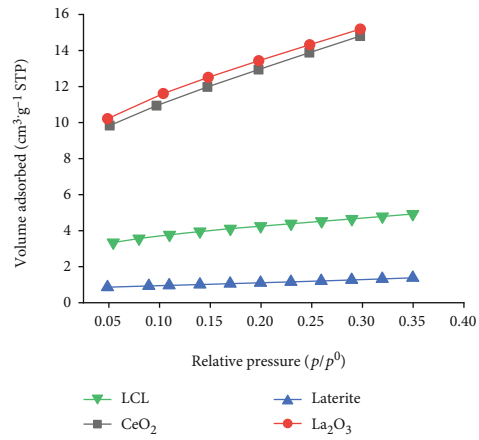

Figure 4: The nitrogen adsorption isotherms of CeO_2, La_2O_3, laterite, and LCL for BET analysis.

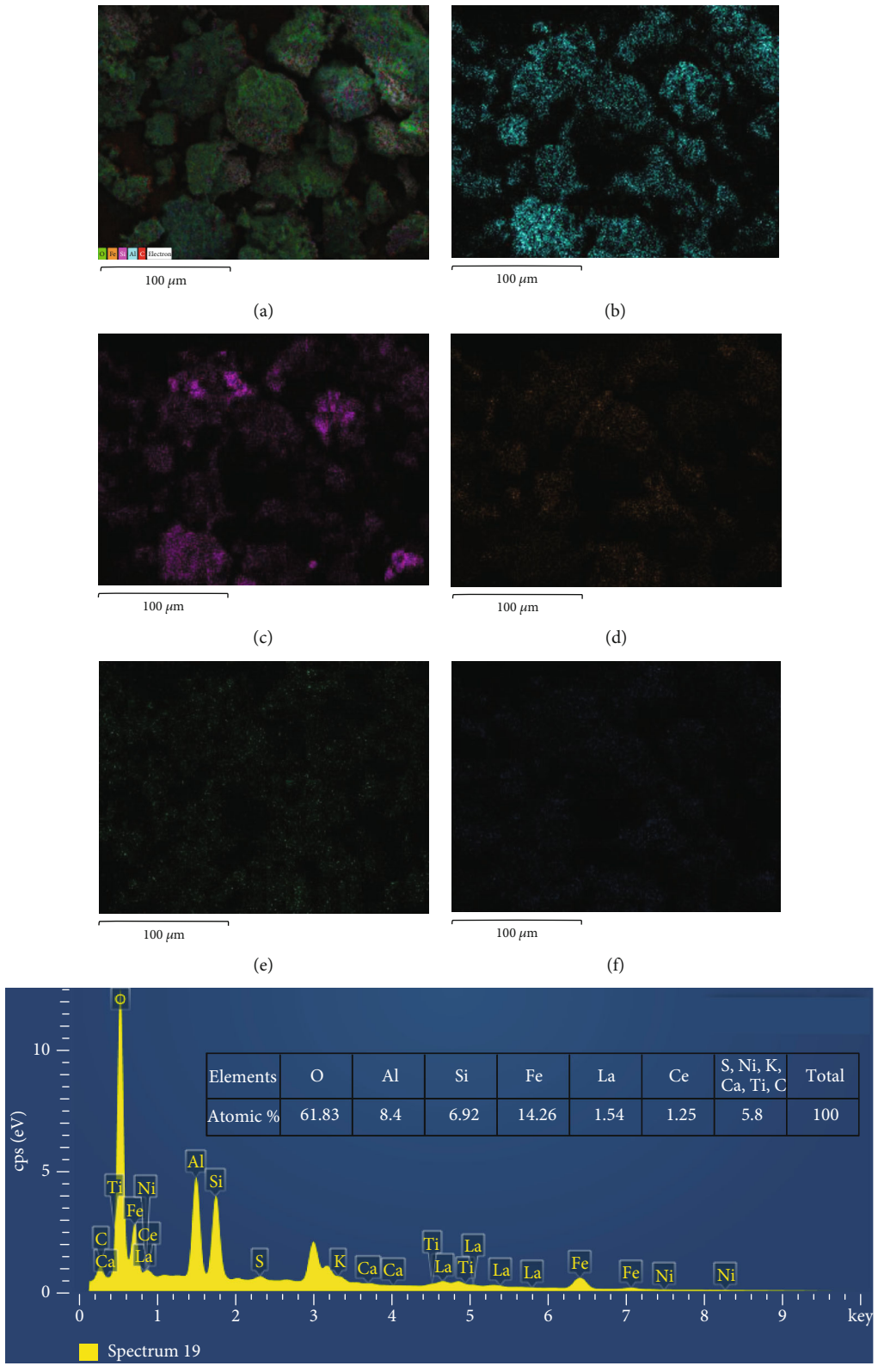

Figure 5: EDX mapping analysis of LCL (a); the mapping distribution of Al element (b); Si element (c); Fe element (d); La element (e); Ce element (f); EDX spectrum of LCL (g).

where K_F is the Freundlich constant, n is the empirical parameter.

The Langmuir isotherm model is expressed as follows [41]:

$$q_e = \frac{K_L \cdot q_m \cdot C_e}{1 + K_L \cdot C_e}, \quad (10)$$

where q_m is the maximum monolayer capacity amount ($mg \cdot g^{-1}$), K_L is the Langmuir equilibrium constant ($L \cdot mg^{-1}$). The model parameters were determined using nonlinear regression.

2.4.2. Desorption of Adsorbents. The saturated NaCl solution was used to recover LCL nanoparticles. A saturated NaCl solution was allowed to run through a column containing the used LCL nanoparticles several times to completely eliminate the adsorbates (fluoride or arsenite). The recovered LCL nanoparticles were separated from the column and cleaned in both acid and base solutions and subsequently dried at 110°C for 12 hours before reuse.

3. Results and Discussion

3.1. Synthesis of La_2O_3-CeO_2/Laterite (LCL). The thermal behavior of LCL is presented in Figure 1. As can be seen from Figure, three distinct weight losses according to three exothermic process peaks at 192°C, 281°C, and 476°C are observed. The two first losses of around 15% are probably attributed to the evaporation of moisture and gelatin with low molecular masses. Nevertheless, major weight losses of about 10% are observed in the range of 400°C-500°C, which corresponds to the decomposition of the main chain of gelatin. Therefore, the temperature of at least 500°C is required to completely remove the gelatin.

The structural phases of the obtained samples were studied by XRD measurement (Figure 2). Figures 2(a) and 2(b) present the characteristic diffractions of lanthanum oxide and cerium oxide according to JCPDS No. 01-072-6356 and JCPDS No. 01-080-6915, respectively. The major constituents of laterite are quartz (JCPDS No. 00-003-0444) and iron oxide (JCPDS No. 01-084-0308). As expected, the LCL pattern exhibited crystallization with characteristic diffraction peaks of lanthanum oxide, cerium oxide, iron oxide hematite (JCPDS No. 01-071-5088), and quartz indicating the formation of the laterite/lanthanum oxide/cerium oxide composite.

The morphology of the obtained samples was performed by SEM observation (Figure 3). Both La_2O_3 and CeO_2 materials exhibit large agglomerates of fine particles of around 50–200 nm. It is clear that laterite exhibits a highly porous structure with a heterogeneous texture. The LCL composite presents the embroiling of fine oxide particles in the laterite matrix.

The specific surface areas of the obtained materials were calculated by the Brunauer–Emmett–Teller (BET) model using adsorption data with relative pressure in the range of 0.05–0.35 (Figure 4). It was found that the specific surface areas of lanthanum oxide, cerium oxide, laterite, and LCL are 47.3, 48.3, 4.0, and 14.4 $m^2 \cdot g^{-1}$, respectively. Laterite exhibits a significantly low surface area, but the combination of laterite with lanthanum and cerium oxides greatly enhances the specific surface area which can lead to an improvement in its adsorption capacity.

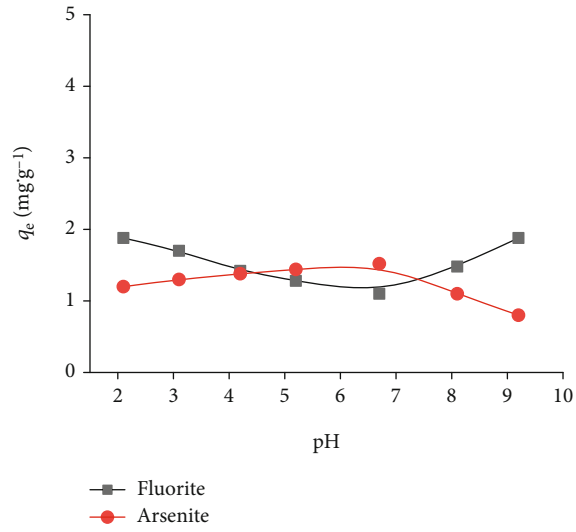

Figure 6: The variation of arsenite and fluoride adsorption capacities of LCL with pH (m_{LCL}: 0.5 g; V: 100 mL; initial conc. is 1 mg·L^{-1} for arsenite and 2 mg·L^{-1} for fluorite; contact time: 120 min; temperature: 25°C).

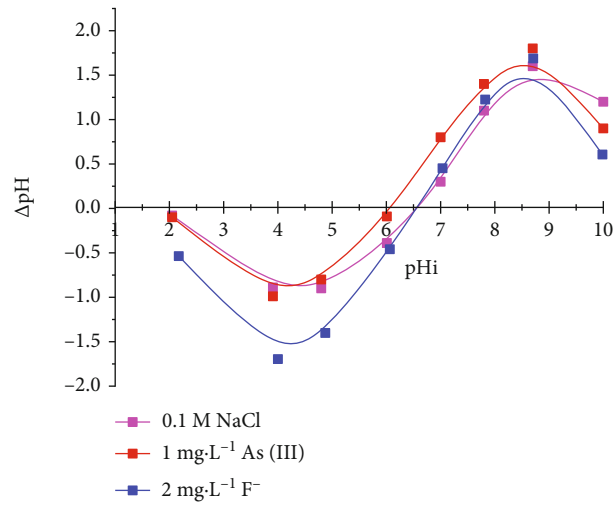

Figure 7: The pH_{PZC} of LCL material in the inert electrolyte and in the presence of arsenite and fluoride (m_{LCL}: 0.5 g; V: 100 mL; initial conc.: 1 mg·L^{-1}).

The element composition of the LCL sample was analyzed by EDX spectroscopy. The main elements include Al, Si, Fe, La, and Ce in laterite and added oxides. It is notable that the La/Ce molar ratio in the product was close to the initial mixture. The distribution of elements in the obtained composite was studied by EDX mapping (Figure 5) showing that elements of Ce and La were highly dispersed in the laterite matrix. Some other elements (S, Mi, K, Ca, Ti, and C) of

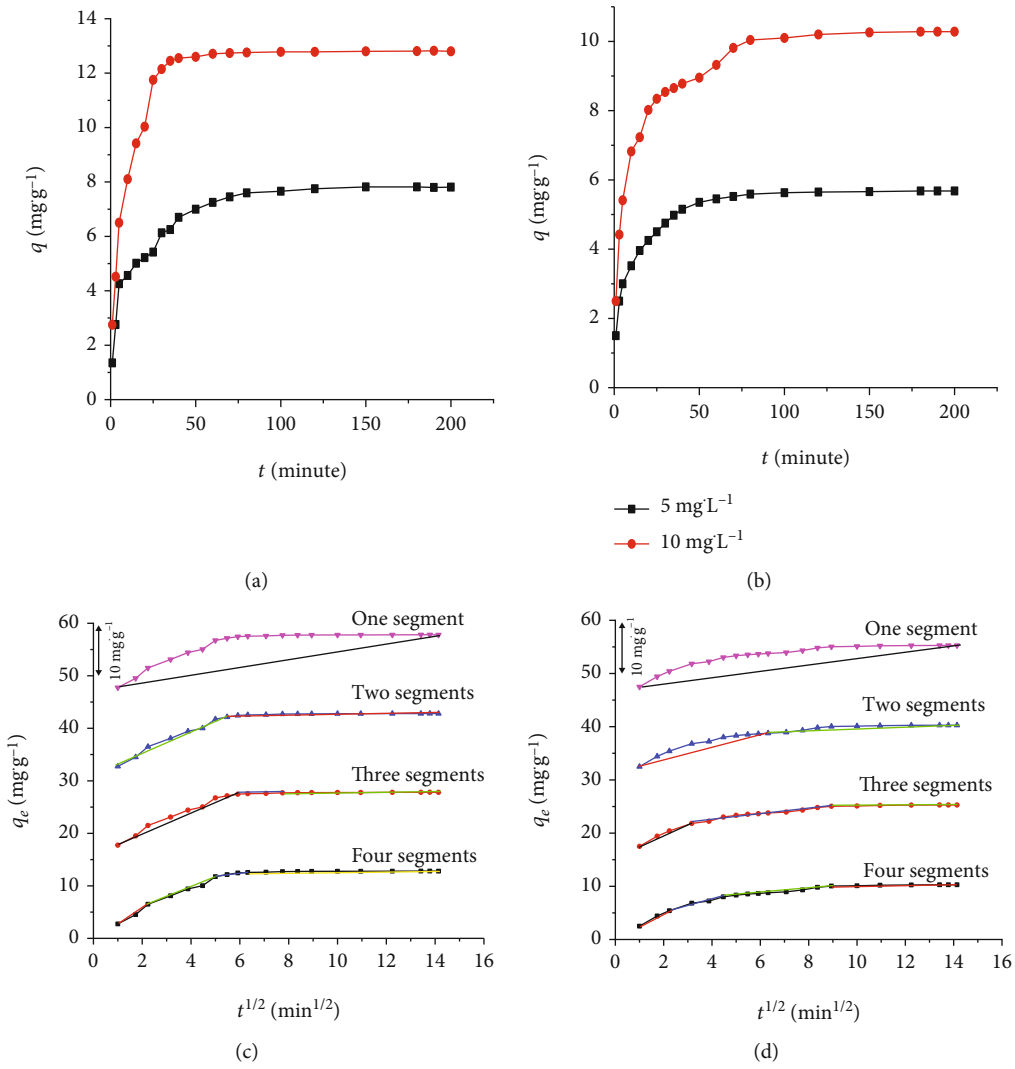

Figure 8: Kinetics of (a) arsenite adsorption and (b) fluoride adsorption at different initial concentrations on LCL. (c) The plot of multilinear regression for arsenite adsorption at 10 mg·L^{-1}. (d) The plot of multilinear regression for fluoride adsorption at 10 mg·L^{-1} (m_{LCL}: 2.5 g; V: 500 mL; initial As(III) concentrations: 5 and 10 mg·L^{-1}; initial F^- concentrations: 5 and 10 mg·L^{-1}).

Table 2: Parameters of formal kinetics for arsenite and fluoride adsorption onto LCL.

Adsorbate	Conc. (mg·L^{-1})	*Pseudo*-first-order model				*Pseudo*-second-order model		
		q_{exp} (mg·g^{-1})	q_{1model} (mg·g^{-1})	k_1 (min^{-1})	R^2	q_{2model} (mg·g^{-1})	k_2 (g·mg^{-1}·min^{-1})	R^2
Arsenite	5	7.82	3.71	$2.3 \cdot 10^{-2}$	0.955	7.97	$1.65 \cdot 10^{-2}$	0.997
	10	12.82	4.40	$3.7 \cdot 10^{-2}$	0.933	13.19	$1.97 \cdot 10^{-2}$	0.999
Fluoride	5	5.68	2.55	$2.14 \cdot 10^{-2}$	0.986	5.72	$2.43 \cdot 10^{-2}$	0.996
	10	10.28	4.93	$3.31 \cdot 10^{-2}$	0.949	10.61	$1.60 \cdot 10^{-2}$	0.996

around 5.8 atomic % as impurities in laterites were found in EDX mapping (data not shown).

3.2. Arsenite and Fluoride Adsorption on La_2O_3/CeO_2/Laterite Composite (LCL)

3.2.1. Effect of pH. The effect of pH on the adsorption of arsenite or fluoride over LCL was investigated in the pH range of 2–9.2 (Figure 6). No significant change in arsenite adsorption capacity was observed in the pH range of 2 to 9.2. This is consistent with the existence of the solely neutral molecule H3AsO3 in aqueous media at pH < 9.2 [42]. Hence, the electrostatic interaction could play a negligible role in the arsenite removal due to uncharged arsenite species at this pH range. The pH_{PZC} of LCL was estimated by the pH drift method [43] (Figure 7). It was notable that the pH_{PZC}

Table 3: Parameter of intraparticle diffusion model for arsenite and fluoride adsorption at different initial concentrations.

C_{As} (mg·L^{-1})	Linear one-segment regression			Linear two-segment regression			Linear three-segment regression			Linear four-segments regression		
	SSE	R^2	AIC	SSE	R^2	AIC	SSE	R^2	AIC	SSE	R^2	AIC
5	28.26	0.566	11.62	8.02	0.88	-7.62	4.20	0,94	-12.77	8.02	0.93	10.01
10	113.05	0.37	39.34	48.62	0.73	28.43	1.30	0,99	-36.23	1.30	0.99	-25.60
C_F^- (mg·L^{-1})	Linear one-segment regression			Linear two-segment regression			Linear three-segment regression			Linear four-segments regression		
	SSE	R^2	AIC	SSE	R^2	AIC	SSE	R^2	AIC	SSE	R^2	AIC
5	13.99	0.51	-2.43	4.59	0.38	-18.76	0.44	0.98	-57.98	4.59	0.89	-0.34
10	41.82	0.53	19.46	11.56	0.87	-0.30	2.10	0.98	-26.61	2.10	0.98	-15.99

Table 4: Piecewise regression analysis for the three-linear-segment model for LCL.

C	First linear segment		Second linear segment		Third linear segment	
Arsenite (mg·L^{-1})	Intercept 1	Slope 1	Intercept 2	Slope 2	Intercept 3	Slope 2
5	-1.058 (-7.43; 5.332)	2.32	2.73 (2.14; 3.32)	0.60	6.30 (5.78; 6.82)	0.12
10	1.41 (0.39; 2.43)	1.998	11.70 (11.12; 12.27)	0.13	12.63 (12.57; 12.68)	0.014
Fluorite (mg·L^{-1})	Intercept 1	Slope 1	Intercept 2	Slope 2	Intercept 3	Slope 2
5	0.31 (-1.96; 2.57)	1.22	2.64 (2.17; 3.12)	0.35	5.51 (5.47; 5.55)	0.012
10	0.77 (-1.12; 2.66)	1.98	5.48 (4.96; 5.99)	0.52	9.65 (9.45; 99.85)	0.047

The values in parentheses describe a 95% confidence interval.

decreases from ~6.6 in a solution without arsenite to ~6.1 in a solution with 1 mg·L^{-1} $NaAsO_2$ (Figure 7). The shift of pH_{PZC} could be due to the result from the negatively charged inner-sphere complexes between arsenite and the adsorbent [44, 45], and effective removal was achieved. Similarly, the fluoride adsorption capacity varies slightly from 1.88 at pH 2 to 1.1 mg·L^{-1} at pH 7 and increases to 1.88 mg·g^{-1} at pH 9.2 (Figure 6). The pH_{PZC} of LCL does not vary much from ~6.6 (in an electrolyte solution) to ~6.5 (with 2 mg·L^{-1} F) (Figure 7). The anionic displacement and adsorption *via* coulombic forces on the surface of metal oxide is widely used to explain the result in the fluoride adsorption of porous materials [40, 41]. However, the electrostatic interaction does not play an important role in this case, and the capillary attraction could explain for the fluoride adsorption of LCL due to its porous structure with a heterogeneous texture.

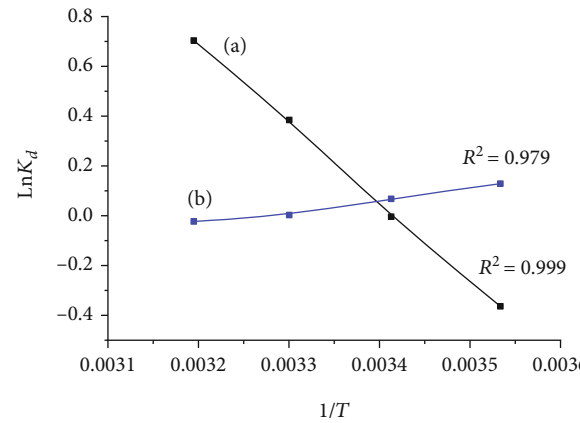

Figure 9: Arrhenius plots of ln K_d *vs.* 1/T for arsenite adsorption (a) and fluoride adsorption (b).

3.2.2. Adsorption Kinetics. The kinetic experiments were conducted at two concentrations of arsenite or fluoride (Figures 8(a) and 8(b)).

More than 90% of arsenite (C_o = 5 mg · L^{-1}) and fluoride (C_o = 10 mg · L^{-1}) were removed within the first 120 min. The adsorption occurred in three distinct stages for both the arsenite and fluoride: (1) a rapid removal in the first 20 min (>50%), (2) relatively slower removal after 20 min until 120 min, and (3) little removal beyond 120 min. The fitting of experimental data to the *pseudo*-first-order and *pseudo*-second-order reaction models shows that the *pseudo*-second-order model provides the best fit ($R^2 > 0.990$) for both arsenite and fluoride (Table 2). The plot of Weber's model in multilinearity was performed. It was found that the three-segment linear model gives the best goodness of fit with the lowest AIC (Table 3 and Figures 8(c) and 8(d)). As seen from Table 3, the intercept of the first segment with 95% confidence interval in the plot varies from a negative value to a positive value (except for 10 mg·L^{-1} of arsenite) (Table 4) indicating that the intercept passes the origin or the intraparticle diffusion is the rate-limiting process. In the second and third stages, all values of the intercept varying from a positive value to a positive value are significantly different from zero

Table 5: Thermodynamic parameters for arsenite and fluoride adsorption.

T (K)	Arsenite adsorption			Fluoride adsorption		
	ΔH° (kJ·mol^{-1})	ΔS° (kJ·Mol^{-1}·K^{-1})	ΔG° (kJ·mol^{-1})	ΔH° (kJ·mol^{-1})	ΔS° (kJ·mol^{-1}·K^{-1})	ΔG° (kJ·mol^{-1})
283	25.87	0.90	0.298	-3.482	-0.011	-0.171
293			– 0.605			-0.337
303			– 1.150			-0.226
313			– 2.412			-0.004

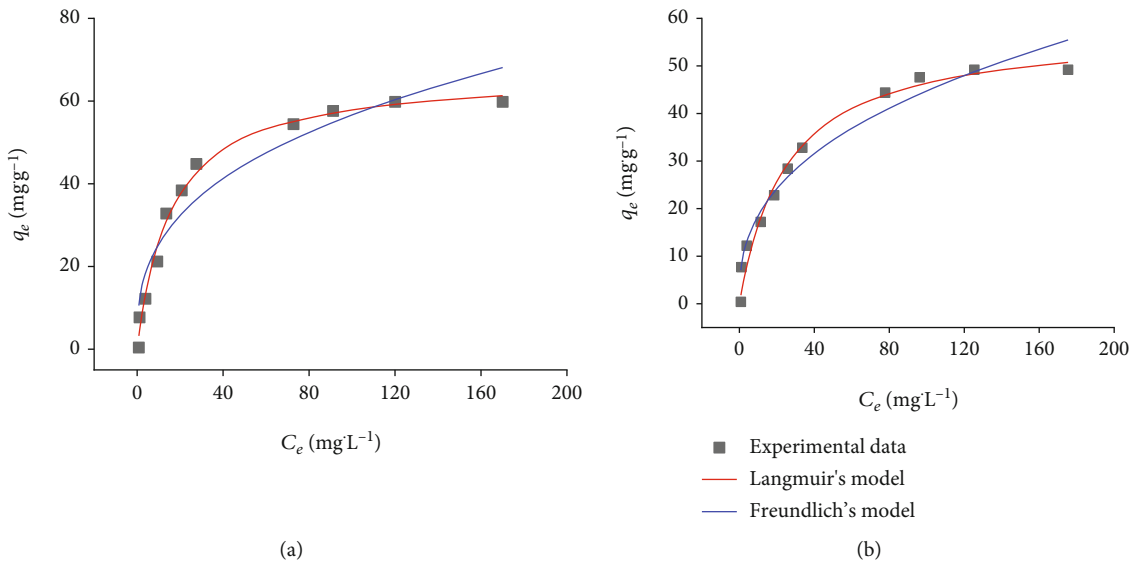

Figure 10: Adsorption equilibrium isotherms of (a) arsenite and (b) fluoride on LCL.

Table 6: Parameters of Langmuir's and Freundlich's isotherm models at 25°C.

		Langmuir's isotherm model			Freundlich's isotherm model		
		q_m (mg·g^{-1})	K_L	R^2	K_F	n	R^2
La_2O_3	Arsenite	89.10	0.112	0.988	20.276	3.359	0.955
	Fluorite	67.83	0.020	0.997	3.761	1.851	0.992
CeO_2	Arsenite	52.54	0.040	0.987	7.235	2.650	0.943
	Fluorite	28.17	0.204	0.991	7.443	3.696	0.964
Laterite	Arsenite	6.34	0.029	0.998	0.679	2.450	0.987
	Fluorite	4.27	0.055	0.998	0.764	3.056	0.985
LCL	Arsenite	67.08	0.063	0.996	11.400	2.873	0.965
	Fluorite	58.02	0.039	0.991	7.702	2.617	0.980

implying that the line does not pass the origin [38]. These results reveal that the intraparticle diffusion is not the only rate-limiting process.

3.2.3. Thermodynamic Parameters. A thermodynamic study was performed in the temperature range of 283–313 K (Figure 9). By increasing temperature from 283 to 313 K, arsenite removal efficiency increases but that for fluoride decreases. At 283 K, arsenite and fluoride adsorption capacities were 8.3 and 10.9 mg·g^{-1}, respectively, and by increasing solution temperature to 313 K, adsorption capacity increases to 13.38 mg·g^{-1} for arsenite but decreases to 10.2 mg·g^{-1} for fluoride. The positive values of ΔH° and ΔS° indicate the endothermic nature and high randomness at the surface of solid/solution phases in the arsenite adsorption system (Table 5). The increase in the randomness may be related to the fact that the displacement of adsorbed water molecules or hydroxyl ion by the arsenite species enhances translational entropy which creates the prevalence of randomness in the system [46]. The low exothermic enthalpy value and negative

Table 7: Comparison of arsenite and fluoride adsorption capacity for various materials with the LCL.

Adsorbent	Specific surface area ($m^2 \cdot g^{-1}$)	q_m ($mg \cdot g^{-1}$)	References
Fluoride			
Aligned carbon nanotubes	75	2.85	[43]
Amorphous alumina supported on carbon nanotubes	165	28.7	[44]
Pumice modified by hydrogen peroxide	53.1	11.8	[45]
Pumice modified by HCl and NaOH	N/A	65.5	[47]
UiO-66-NH_2	905	58.8	[46]
LCL	14.4	58.02	The present work
Arsenite			
Iron nanoparticles/graphene oxide	160	306	[37]
Layered double hydroxide biochars	N/A	16.1	[48]
Hydrous cerium oxide (HCO) nanoparticles	198	172	[27]
Laterite	15.4	0.18	[49]
Acidified laterite	99.36	1.90	[50]
LCL	14.4	67.08	The present work

Table 8: Effect of competing ions on arsenite and fluorite adsorption of LCL (C_0 (arsenite) = 5 mg · L^{-1}; C_0 (fluoride) = 10 mg · L^{-1}; V = 100 mL; m_{LCL} = 0.5 g).

Interferent ions	Arsenite adsorption		Fluoride adsorption	
	Molar ratio[a]	q ($mg \cdot g^{-1}$)	Molar ratio[a]	q ($mg \cdot g^{-1}$)
Fe(III)	0	3.14	0	8.84
	1	3.18	1	9.1
	1.4	3.28	10	15.84
	2	3.38	20	16.2
Mn(II)	0	3.14	0	8.3
	1	3.16	1	8.42
	1.4	3.2	10	9.04
	2	3.22	20	10.08
Cl-	0	3.14	0	8.30
	10	2.76	1	8.30
	20	2.16	10	8.28
	50	1.84	20	8.30
SO_4^{2-}	0	3.14	0	8.30
	10	2.88	1	8.26
	20	2.62	10	8.26
	40	2.04	40	8.26

"a" indicates the interferent/adsorbate molar ratio.

entropy change in fluoride adsorption imply the possible domination of physical forces. However, the negative Gibbs free energy indicates the spontaneous process of arsenite or fluoride adsorption at the studied temperature range.

3.2.4. Adsorption Equilibrium. Langmuir and Freundlich isotherm models were employed to estimate arsenite and fluoride sorption behavior by LCL. Both arsenite and fluoride adsorption data were found to be fitted better for the Langmuir model (R^2 = 0.99 and 0.99 for arsenite and fluoride, respectively) than the Freundlich model (R^2 = 0.96 and 0.98 for arsenite and fluoride, respectively) (Figure 10).

Based on the Langmuir isotherm, the maximum monolayer capacity amount of LCL was found to be 67.08 $mg \cdot g^{-1}$ for arsenite and 58.02 $mg \cdot g^{-1}$ for fluoride (Table 6). It was notable that laterite has low arsenite or fluoride adsorption. However, the combination of laterite with oxides significantly increases the adsorption capacity. Although the arsenite and fluoride adsorption capacity of LCL is lower than the lanthanum oxide and cerium oxides, they are compatible

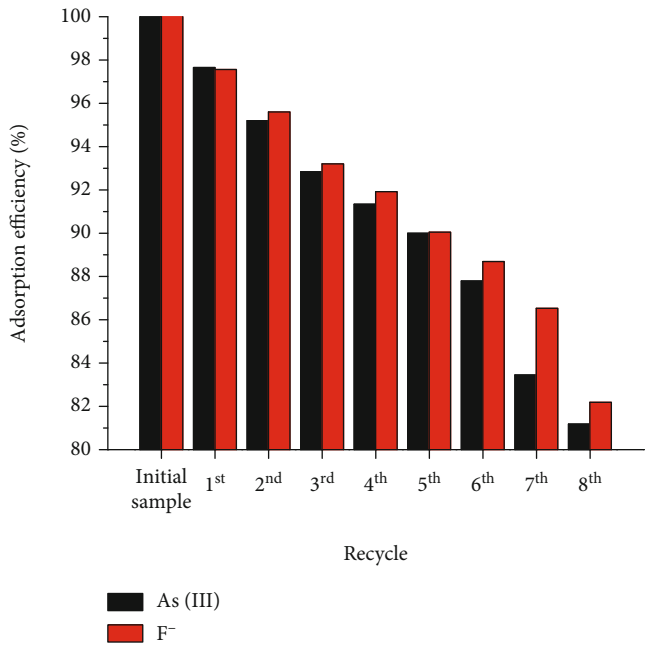

Figure 11: Adsorption capacity of arsenite and fluoride on LCL after each reuse.

compared to other materials so far reported as shown in Table 7. Since the laterite natural mineral is inexpensive, the high adsorption capacity makes it a great potential adsorbent for the removal of arsenite and fluoride from aqueous sources.

3.2.5. Competing Anions. The arsenite or fluoride removal performance in the presence of Fe(III), Mn(II), Cl-, and SO_4^{2-} was conducted with the initial concentrations of arsenite and fluoride of 5 mg·L^{-1} and 10 mg·L^{-1}, respectively (Table 8). It was found that in the presence of 2-fold excess of iron (III), the adsorption capacity for arsenite improved from 3.14 to 3.38 mg·g^{-1} and that for fluoride almost doubled from 8.84 to 16.2 mg·g^{-1} with 10-fold excess of iron (III). Mn(II) also slightly enhanced the arsenite and fluoride removal ability of LCL. The anions such as Cl^- and SO_4^{2-} did not show any observable effect on the adsorption of fluoride; however, that of arsenate was reduced by half in the presence of 20-fold excess of Cl^-, and by one-third in the presence of 40-fold excess of SO_4^{2-}.

3.2.6. Reusability. The reusability of LCL is one of the important criteria for its practical applications. The arsenite or fluoride amount adsorbed on LCL was desorbed with a NaCl-saturated solution. Before reuse, the recycled LCL was dried at 110°C for 12 h. After eight cycles, the adsorption capacity declines by approximately 8% for arsenite and 10% for fluoride (Figure 11) indicating that LCL was stable after several adsorption cycles.

4. Conclusions

Laterite has been effectively used as a matrix material carrying La-Ce binary oxides to form efficient adsorbents. The La_2O_3-CeO_2/laterite exhibits high fluoride and arsenite removal efficiency in a wide pH range. The combination of laterite with lanthanum and cerium oxides enhances significantly the arsenite and fluoride adsorption capacity compared with laterite. The arsenite and fluoride adsorption capacity of the La_2O_3-CeO_2/laterite are 10.5 and 13.6 times higher than those of laterite, respectively. It is a promising adsorbent due to the high recyclability and arsenite and fluoride adsorption capacity. The easy availability and abundance of laterite in various areas in Vietnam make LCL an inexpensive, feasible, and applicable material in practice.

Data Availability

The data used to support the findings of this study are available from the corresponding author upon request.

Conflicts of Interest

The authors declare that they have no conflicts of interest.

Acknowledgments

This study was financially supported by the Vietnam Academy of Science and Technology through grant number UQĐTCB.02/20-21.

Supplementary Materials

A statistical approach of the piecewise linear regression combined with Akaike's information criteria (AIC) for the analysis of kinetics data. This method allows the determination of the number of linear segments and the nature of each one, which would avoid the subjective decisions that are common with the graphical method. AIC is employed to compare the models. AIC estimates how well the data support each model. The model with the lowest AIC_c score is most likely the correct model. *(Supplementary Materials)*

References

[1] M. Amini, K. Mueller, K. C. Abbaspour et al., "Statistical modeling of global geogenic fluoride contamination in groundwaters," *Environmental Science & Technology*, vol. 42, no. 10, pp. 3662–3668, 2008.

[2] M. Bissen and F. H. Frimmel, "Arsenic—a review. Part I: occurrence, toxicity, speciation, mobility," *Acta hydrochimica et hydrobiologica*, vol. 31, no. 1, pp. 9–18, 2003.

[3] S. Ayoob and A. K. Gupta, "Fluoride in drinking water: a review on the status and stress effects," *Critical Reviews in Environmental Science and Technology*, vol. 36, no. 6, pp. 433–487, 2006.

[4] D. Mohan and C. U. Pittman Jr., "Arsenic removal from water/wastewater using adsorbents—a critical review," *Journal of Hazardous Materials*, vol. 142, no. 1-2, pp. 1–53, 2007.

[5] M. A. Malana, R. B. Qureshi, and M. N. Ashiq, "Adsorption studies of arsenic on nano aluminium doped manganese copper ferrite polymer (MA, VA, AA) composite: kinetics and mechanism," *Chemical Engineering Journal*, vol. 172, no. 2-3, pp. 721–727, 2011.

[6] USEPA, "National primary drinking water regulations; arsenic and clarifications to compliance and new source contaminants monitoring," *Federal Register*, vol. 66, no. 6975, 2001.

[7] G. WHO, "Guidelines for drinking-water quality," *World Health Organazation*, vol. 216, pp. 303-304, 2011.

[8] Y. Chen, F. Parvez, M. Gamble et al., "Arsenic exposure at low-to-moderate levels and skin lesions, arsenic metabolism, neurological functions, and biomarkers for respiratory and cardiovascular diseases: review of recent findings from the Health Effects of Arsenic Longitudinal Study (HEALS) in Bangladesh," *Toxicology and Applied Pharmacology*, vol. 239, no. 2, pp. 184–192, 2009.

[9] D. R. Lide, *CRC Handbook of Chemistry and Physics*, CRC press, Boca Raton, Florida, USA, 2004.

[10] N. J. Chinoy, "Effects of fluoride on physiology of animals and human beings," *Indian Journal of Environment and Toxicology*, vol. 1, pp. 17–32, 1991.

[11] M. Hichour, F. Persin, J. Molénat, J. Sandeaux, and C. Gavach, "Fluoride removal from diluted solutions by Donnan dialysis with anion-exchange membranes," *Desalination*, vol. 122, no. 1, pp. 53–62, 1999.

[12] M. Hichour, F. Persin, J. Sandeaux, and C. Gavach, "Fluoride removal from waters by Donnan dialysis," *Separation and Purification Technology*, vol. 18, no. 1, pp. 1–11, 1999.

[13] O. X. Leupin and S. J. Hug, "Oxidation and removal of arsenic (III) from aerated groundwater by filtration through sand and zero-valent iron," *Water Research*, vol. 39, no. 9, pp. 1729–1740, 2005.

[14] T. Nishimura and Y. Umetsu, "Oxidative precipitation of arsenic (III) with manganese (II) and iron (II) in dilute acidic solution by ozone," *Hydrometallurgy*, vol. 62, no. 2, pp. 83–92, 2001.

[15] H. K. Hansen, P. Núñez, and R. Grandon, "Electrocoagulation as a remediation tool for wastewaters containing arsenic," *Minerals Engineering*, vol. 19, no. 5, pp. 521–524, 2006.

[16] K. Košutić, L. Furač, L. Sipos, and B. Kunst, "Removal of arsenic and pesticides from drinking water by nanofiltration membranes," *Separation and Purification Technology*, vol. 42, no. 2, pp. 137–144, 2005.

[17] T. Urase, J. Oh, and K. Yamamoto, "Effect of pH on rejection of different species of arsenic by nanofiltration," *Desalination*, vol. 117, no. 1-3, pp. 11–18, 1998.

[18] K. Vaaramaa and J. Lehto, "Removal of metals and anions from drinking water by ion exchange," *Desalination*, vol. 155, no. 2, pp. 157–170, 2003.

[19] B. An, T. R. Steinwinder, and D. Zhao, "Selective removal of arsenate from drinking water using a polymeric ligand exchanger," *Water Research*, vol. 39, no. 20, pp. 4993–5004, 2005.

[20] B. Han, T. Runnells, J. Zimbron, and R. Wickramasinghe, "Arsenic removal from drinking water by flocculation and microfiltration," *Desalination*, vol. 145, no. 1-3, pp. 293–298, 2002.

[21] T. Ruiz, F. Persin, M. Hichour, and J. Sandeaux, "Modelisation of fluoride removal in Donnan dialysis," *Journal of Membrane Science*, vol. 212, no. 1-2, pp. 113–121, 2003.

[22] X. Xu, Q. Li, H. Cui et al., "Adsorption of fluoride from aqueous solution on magnesia-loaded fly ash cenospheres," *Desalination*, vol. 272, no. 1-3, pp. 233–239, 2011.

[23] A. Maiti, S. DasGupta, J. K. Basu, and S. De, "Adsorption of arsenite using natural laterite as adsorbent," *Separation and Purification Technology*, vol. 55, no. 3, pp. 350–359, 2007.

[24] O. Abollino, M. Aceto, M. Malandrino, C. Sarzanini, and E. Mentasti, "Adsorption of heavy metals on Na-montmorillonite. Effect of pH and organic substances," *Water Research*, vol. 37, no. 7, pp. 1619–1627, 2003.

[25] Z. Liu, F.-S. Zhang, and R. Sasai, "Arsenate removal from water using Fe_3O_4-loaded activated carbon prepared from waste biomass," *Chemical Engineering Journal*, vol. 160, no. 1, pp. 57–62, 2010.

[26] Z. Xu, Q. Li, S. Gao, and J. K. Shang, "As (III) removal by hydrous titanium dioxide prepared from one-step hydrolysis of aqueous $TiCl_4$ solution," *Water Research*, vol. 44, no. 19, pp. 5713–5721, 2010.

[27] S. R. Kanel, J.-M. Greneche, and H. Choi, "Arsenic (V) removal from groundwater using nano scale zero-valent iron as a colloidal reactive barrier material," *Environmental Science & Technology*, vol. 40, no. 6, pp. 2045–2050, 2006.

[28] G. Zhang, S. Wu, Y. Li, and Q. Zhang, "Significant improvement in activity, durability, and light-to-fuel efficiency of Ni nanoparticles by La_2O_3 cluster modification for photothermocatalytic CO_2 reduction," *Applied Catalysis B: Environmental*, vol. 264, 2020.

[29] Y. Yulizar, E. Kusrini, D. O. B. Apriandanu, and N. Nurdini, "*Datura metel* L. leaves extract mediated CeO_2 nanoparticles: synthesis, characterizations, and degradation activity of DPPH radical," *Surfaces and Interfaces*, vol. 19, 2020.

[30] A. Umar, A. A. Ibrahim, R. Kumar et al., "Fern shaped La_2O_3 nanostructures as potential scaffold for efficient hydroquinone chemical sensing application," *Ceramics International*, vol. 46, no. 4, pp. 5141–5148, 2020.

[31] A. Y. Estevez and J. S. Erlichman, "The potential of cerium oxide nanoparticles (nanoceria) for neurodegenerative disease therapy," *Nanomedicine*, vol. 9, no. 10, pp. 1437–1440, 2014.

[32] R. Li, Q. Li, S. Gao, and J. K. Shang, "Exceptional arsenic adsorption performance of hydrous cerium oxide nanoparticles: Part A. Adsorption capacity and mechanism," *Chemical Engineering Journal*, vol. 185, pp. 127–135, 2012.

[33] B. Wu and I. M. C. Lo, "Surface functional group engineering of CeO_2 particles for enhanced phosphate adsorption," *Environmental Science & Technology*, vol. 54, no. 7, pp. 4601–4608, 2020.

[34] H. Guo, J. Chen, W. Weng, Z. Zheng, and D. Wang, "Adsorption behavior of Congo red from aqueous solution on La_2O_3-doped TiO_2 nanotubes," *Journal of Industrial and Engineering Chemistry*, vol. 20, no. 5, pp. 3081–3088, 2014.

[35] Y. S. Ho, D. A. J. Wase, and C. Forster, "The adsorption of divalent copper ions from aqueous solution by sphagnum moss peat," *Equilibrium*, vol. 260, pp. 150–200, 1994.

[36] S. Lagergren, "Theorie der Sogenannten Adsorption Geloster Stoffe. Stockholm. Bihang till. K," *Bihang till Kungliga Svenska Vetenskapsakademiens, Handlingar*, vol. 24, pp. 1–39, 1898.

[37] W. J. Weber and J. C. Morris, "Advances in water pollution research: removal of biologically resistant pollutant from waste water by adsorption," in *Proceedings of 1st International Conference on Water Pollution Symposium*, 1962.

[38] G. F. Malash and M. I. El-Khaiary, "Piecewise linear regression: a statistical method for the analysis of experimental adsorption data by the intraparticle-diffusion models," *Chemical Engineering Journal*, vol. 163, no. 3, pp. 256–263, 2010.

[39] R. Han, J. Zhang, W. Zou, J. Shi, and H. Liu, "Equilibrium biosorption isotherm for lead ion on chaff," *Journal of Hazardous Materials*, vol. 125, no. 1-3, pp. 266–271, 2005.

[40] H. Freundlich, "Uber die adsorption in lasungen," *The Journal of Physical Chemistry*, vol. 57, p. 385, 1906.

[41] I. Langmuir, "The constitution and fundamental properties of solids and liquids. Part I. Solids," *Journal of the American Chemical Society*, vol. 38, no. 11, pp. 2221–2295, 1916.

[42] T. K. Das, T. S. Sakthivel, A. Jeyaranjan, S. Seal, and A. N. Bezbaruah, "Ultra-high arsenic adsorption by graphene oxide iron nanohybrid: removal mechanisms and potential applications," *Chemosphere*, vol. 253, 2020.

[43] Y. Jiao, D. Han, Y. Lu et al., "Characterization of pine-sawdust pyrolytic char activated by phosphoric acid through microwave irradiation and adsorption property toward CDNB in batch mode," *Desalination and Water Treatment*, vol. 77, pp. 247–255, 2017.

[44] M. E. Pena, G. P. Korfiatis, M. Patel, L. Lippincott, and X. Meng, "Adsorption of As(V) and As(III) by nanocrystalline titanium dioxide," *Water Research*, vol. 39, no. 11, pp. 2327–2337, 2005.

[45] R. Chitrakar, S. Tezuka, A. Sonoda, K. Sakane, K. Ooi, and T. Hirotsu, "Phosphate adsorption on synthetic goethite and akaganeite," *Journal of Colloid and Interface Science*, vol. 298, no. 2, pp. 602–608, 2006.

[46] M. Doula, A. Ioannou, and A. Dimirkou, "Thermodynamics of copper adsorption-desorption by Ca-kaolinite," *Adsorption*, vol. 6, no. 4, pp. 325–335, 2000.

[47] M. G. Sujana and S. Anand, "Iron and aluminium based mixed hydroxides: a novel sorbent for fluoride removal from aqueous solutions," *Applied Surface Science*, vol. 256, no. 23, pp. 6956–6962, 2010.

[48] Y.-H. Li, S. Wang, X. Zhang et al., "Adsorption of fluoride from water by aligned carbon nanotubes," *Materials Research Bulletin*, vol. 38, no. 3, pp. 469–476, 2003.

[49] Y.-H. Li, S. Wang, A. Cao et al., "Adsorption of fluoride from water by amorphous alumina supported on carbon nanotubes," *Chemical Physics Letters*, vol. 350, no. 5-6, pp. 412–416, 2001.

[50] M. N. Sepehr, V. Sivasankar, M. Zarrabi, and M. Senthil Kumar, "Surface modification of pumice enhancing its fluoride adsorption capacity: an insight into kinetic and thermodynamic studies," *Chemical Engineering Journal*, vol. 228, pp. 192–204, 2013.